JOURNAL OF SOLID STATE CHEMISTRY **133,** 555–567 (1997)
ARTICLE NO. SC977531

High-Temperature Coulometric Titration of $La_{1-x}Sr_xCoO_{3-\delta}$: Evidence for the Effect of Electronic Band Structure on Nonstoichiometry Behavior

Martijn H. R. Lankhorst, H. J. M. Bouwmeester,[1] and H. Verweij

Laboratory of Inorganic Materials Science, Department of Chemical Technology, University of Twente, PO Box 217, 7500 AE Enschede, The Netherlands

Received February 14, 1997; in revised form June 26, 1997; accepted June 30, 1997

The equilibrium oxygen chemical potential and the partial energy and entropy of O_2 in perovskites $La_{1-x}Sr_xCoO_{3-\delta}$ were measured as a function of δ and x by high-temperature oxygen coulometric titration. An almost linear decrease in the oxygen chemical potential is observed with increasing net electron concentration $2\delta-x$. The observed behavior is interpreted to reflect the corresponding increase in the Fermi level on filling up states in a broad electron band with electrons induced by vacancy formation or reducing the Sr-dopant level. The results enable calculation of the apparent density of states at the Fermi level. For low values of δ and high temperatures, the oxygen vacancies in $La_{1-x}Sr_xCoO_{3-\delta}$ are randomly distributed among equivalent oxygen sites. By increasing δ or by lowering the temperature, additional ionic contributions to the partial energy and entropy arise, but these cancel in the chemical potential of oxygen vacancies. These results are possibly due to ordering of oxygen vacancies into microdomains.

1. INTRODUCTION

$La_{1-x}Sr_xCoO_{3-\delta}$ perovskite-type oxides are characterized by their ability to permit relatively large values of the nonstoichiometry parameter δ at elevated temperatures. It is generally accepted that the oxygen nonstoichiometry in these compounds is associated with the formation of lattice oxygen vacancies which have a valency of $2+$ relative to the oxygen sublattice. Charge neutrality requires that the formation of lattice oxygen vacancies is accompanied by a corresponding change in the average valency of either the cobalt or oxygen ions. The high concentration of oxygen vacancies in conjunction with their relatively high mobility cause these materials to exhibit high oxygen ion conductivity, the value of which may be one to two orders of magnitude higher than that of stabilized zirconia. The electronic conductivity is even higher and is metallic-like at high temperatures. Due to the mixed conductivity, these materials are permeable for oxygen gas. Advantageous use can be made as gas separation membranes (1, 2), oxidation catalysts (3), and electrodes in, e.g., solid oxide fuel cells and oxygen sensors (2). An obvious consideration for the design of the applications just mentioned is to understand how the extent of oxygen nonstoichiometry depends on dopant level and environmental parameters like oxygen partial pressure and temperature.

The oxygen nonstoichiometry in $La_{1-x}Sr_xCoO_{3-\delta}$ has been measured as a function of oxygen partial pressure and temperature by Mizusaki *et al.* (4) using thermogravimetry and by Petrov *et al.* (5) using coulometric titration. However, no quantitative models have emerged from these studies. An advantage of the coulometric titration technique is that it permits direct control of the oxygen stoichiometry of the sample specimen, allowing accurate determination of thermodynamic quantities such as the partial energy and entropy associated with oxygen incorporation into the oxide (6, 7).

In a previous paper from this laboratory (8), oxygen coulometric titration was applied to study the thermodynamics of oxygen incorporation into $La_{0.8}Sr_{0.2}CoO_{3-\delta}$. The results were interpreted in terms of a nonstoichiometry model referred to as the itinerant electron model. In this model, oxygen vacancies are assumed to be randomly distributed among equivalent sites, and the conduction electrons are delocalized, occupying energy levels in a partially filled, rigid electron band. With vacancy formation the electron occupancy of the band increases, which results in an upward shift of the Fermi level and a corresponding decrease in the oxygen chemical potential. The itinerant electron behavior is in agreement with the high electronic conductivities and low Seebeck coefficients observed for these compounds (9, 10). On the other hand, experimental data on oxygen nonstoichiometry and electrical conductivity of compounds $La_{1-x}Sr_xFeO_{3-\delta}$ and $La_{1-x}Sr_xCrO_{3-\delta}$ have been successfully modeled assuming that the transition metal ions show charge disproportionation among three

[1] To whom correspondence should be addressed.

0022-4596/97 $25.00

different valence states (11). Applying charge disproportionation to model experimental data of oxygen nonstoichiometry and Seebeck coefficient of $La_{0.8}Sr_{0.2}CoO_{3-\delta}$ led to inconsistent results (8). It may further be noted that charge disproportionation could not be observed in $LaCoO_{3-\delta}$ by means of XAS (12).

This study is aimed at investigating the applicability of the itinerant electron model to other members of the $La_{1-x}Sr_xCoO_{3-\delta}$ series. Therefore, the oxygen nonstoichiometry and the partial energy and entropy of O_2 were measured for $La_{0.6}Sr_{0.4}CoO_{3-\delta}$ and $La_{0.3}Sr_{0.7}CoO_{3-\delta}$ using high-temperature oxygen coulometric titration. The results are compared with data reported previously for $La_{0.8}Sr_{0.2}CoO_{3-\delta}$ (8).

2. THEORY

2.1. Oxygen Coulometric Titration

In a high-temperature oxygen coulometric titration experiment the oxide sample is enclosed in a sealed electrochemical cell. The oxygen stoichiometry of the sample is adjusted by electrochemically pumping oxygen into or out of the cell using a solid electrolyte. The oxygen chemical potential of the sample inside the sealed compartment $\mu_{O_2}^{oxide}$ is determined from the EMF measured across an auxiliary electrolyte using identical metallic probes,

$$\mu_{O_2}^{oxide} = \mu_{O_2}^{ref.} - 4F \times EMF, \qquad [1]$$

where F is Faraday's constant and $\mu_{O_2}^{ref.}$ the oxygen chemical potential of the reference gas (e.g., air). It should be noted that Eq. [1] is valid only at equilibrium, in which case $\mu_{O_2}^{oxide}$ is equal to the oxygen chemical potential of the gas surrounding the sample, $\mu_{O_2}^{gas}$. The value of $\mu_{O_2}^{ref.}$ can be calculated by substituting the values of the oxygen partial pressure and temperature into Eq. [A1] given in the Appendix. When the above procedure to determine $\mu_{O_2}^{oxide}$ is performed as a function of temperature at constant oxygen stoichiometry of the sample, the entropy part $s_{O_2}^{oxide}$ of $\mu_{O_2}^{oxide}$, given by (7)

$$s_{O_2}^{oxide} = -\left(\frac{\partial \mu_{O_2}^{oxide}}{\partial T}\right)_{\delta}, \qquad [2]$$

can be evaluated. The energy part $\varepsilon_{O_2}^{oxide}$ is calculated from $\mu_{O_2}^{oxide} = \varepsilon_{O_2}^{oxide} - T s_{O_2}^{oxide}$.

Electrochemical pumping of oxygen is generally performed using either galvanostatic or potentiostatic methods (13). Both methods allow evaluation of the change in oxygen nonstoichiometry of the sample $\Delta\delta$ by integration of the current I over time,

$$\Delta\delta = \frac{M}{m}\int_{t=0}^{t=\infty} \frac{I(t) - I_{leak}}{2F}\,dt \qquad [3]$$

where I_{leak} is the unavoidable leakage current, m the mass of the sample, and M the molar mass of the oxide material. The potentiostatic method allows easy determination of I_{leak} by measuring the value to which the current decays after a potentiostatic step. In the galvananostatic method, I_{leak} can be calculated from the change in EMF with time when the sample is in equilibrium with the surrounding gas.

2.2. Itinerant Electron Model

In the itinerant electron model it is assumed that the conduction electrons, e', created during oxygen vacancy formation are donated to electron states of a partially filled electron band. Using Kröger–Vink notation (14), the oxidation reaction can be written as

$$O_2^{gas} + 2V_O^{\cdot\cdot} + 4e \rightleftarrows 2O_O^x \qquad [4]$$

where $V_O^{\cdot\cdot}$ denotes oxygen vacancies and O_O^x regular lattice oxygen ions. From this reaction it is seen that pumping oxygen into the oxide lattice leads to changes in both the lattice oxygen vacancy and the itinerant electron concentration. The equilibrium condition for reaction [4] is given by

$$\mu_{O_2}^{oxide} + 2(\mu_{V_O^{\cdot\cdot}} - \mu_{O_O^x}) + 4\mu_{e'} = 0, \qquad [5]$$

where μ_i denotes the chemical potential of species i. Assuming oxygen vacancies and regular lattice oxygen ions are distributed randomly among equivalent oxygen sites and do not interact, it is allowed to use chemical potentials of the type (7, 15)

$$\mu_k = \mu_k^0 + RT \ln([k]), \qquad [6]$$

where μ_k is the chemical potential of the kth structure element and $[k]$ the mole fraction of the kth structure element. By definition the mole fraction of oxygen vacancies $[V_O^{\cdot\cdot}]$ is equal to the oxygen nonstoichiometry δ.

Taking the electron band to be rigid on filling with electrons, an expression can be derived that relates $\mu_{e'}$ to the electron occupancy $[e']$ and density of states at the Fermi level, $g(\varepsilon_F)$ (8),

$$\mu_{e'}([e']) = \mu_{e'}([e'] = [e']^0) + \frac{([e'] - [e']^0)}{g(\varepsilon_F)}, \qquad [7]$$

where $[e']^0$ is defined as the electron occupancy at zero vacancy concentration and zero Sr-dopant level. In Eq. [7], we have neglected the entropy of electrons by assuming that the electron band is very broad. The latter is supported by the low Seebeck coefficients measured for these compounds (9). The Fermi level moves upward as electrons created by vacancy formation or by reducing the Sr-dopant level are donated to the band. The rate at which the Fermi level varies is determined by the density of states at the Fermi

level. This model, which relates variations in the Fermi level to changes in the concentration of ionized defects, is commonly referred to as electron gas rigid band model (electron gas RBM) (16). Although in this model important features like screening, electron correlation, and exchange are neglected, the observed chemical potential variations for alkali metal intercalated transition metal dichalcogenides have been found to correlate well with density of states calculations (17) and data from X-ray absorption measurements (18).

McKinnon and Selwyn (19) criticized the validity of the electron gas RBM. Referring to the screened impurity RBM developed by Friedel (20) to explain the electronic structure of alloys, these authors proposed that when an ionized defect is added, the entire band shifts due to the perturbation constituted by the screened coulomb potential of the defect. Since this shift is exactly opposite that in the Fermi level, expected from the change in electron occupancy, the position of the Fermi level remains unaffected. As discussed by Sellmyer (16) both models lead to the same result for an experiment in which energies are measured relative to the bottom of the band. However, in the present study energies are measured on an absolute scale and therefore the results depend on which model applies to compounds $La_{1-x}Sr_xCoO_{3-\delta}$. The influence of adding a donor impurity to the solid on the position of the electron band and the Fermi level is shown schematically in Fig. 1.

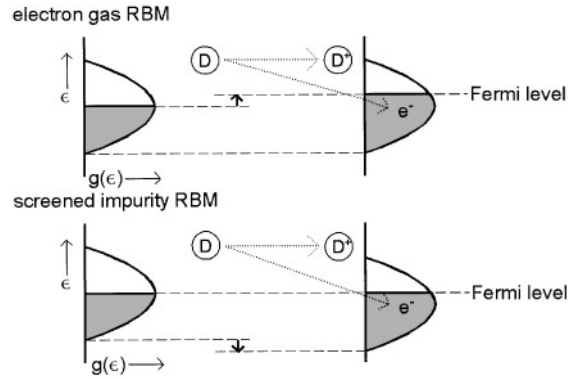

FIG. 1. Schematic plot of the change in position of the electron band and the Fermi level caused by adding a donor to the solid in two versions of the rigid band model. In the electron gas RBM the additional electron leads to an upward shift of the Fermi level while the remaining D^+ ion is supposed to be noninteracting. In the screened impurity RBM the upward shift of the Fermi level is balanced by a downward shift of the entire electron band as a result of coulombic interactions between the electrons and the screened D^+ ion.

An expression for the equilibrium between the oxide and oxygen in the gas phase can be formulated by combining Eqs. [5]–[7] with the charge neutrality condition $[e'] - [e']^0 = 2[V_O^{\cdot\cdot}] - x$. The result is

$$E_{ox} - \frac{4(2[V_O^{\cdot\cdot}] - x)}{g(\varepsilon_F)} - TS_{ox} - 2RT \ln\left(\frac{[V_O^{\cdot\cdot}]}{(3 - [V_{\ddot{o}}])}\right) = \mu_{O_2}^{oxide} = \mu_{O_2}^{gas}, \quad [8]$$

where use has been made of $[O_O^x] = 3 - [V_O^{\cdot\cdot}]$. When the constants in Eq. [8], i.e., E_{ox}, S_{ox}, and the density of states at the Fermi level $g(\varepsilon_F)$ are known, this equation can be used to evaluate the oxygen vacancy concentration as function of oxygen partial pressure and temperature.

From Eqs. [2] and [8] it follows that

$$s_{O_2}^{oxide} = S_{ox} + 2R \ln\left(\frac{[V_O^{\cdot\cdot}]}{3 - [V_O^{\cdot\cdot}]}\right). \quad [9]$$

It is emphasized once more that the electron entropy is assumed to be negligible. The energy of oxygen incorporation is given by

$$\varepsilon_{O_2}^{oxide} = E_{ox} - \frac{4(2[V_O^{\cdot\cdot}] - x)}{g(\varepsilon_F)}. \quad [10]$$

It is recognized that in the itinerant electron model changes in $\varepsilon_{O_2}^{oxide}$ originate from changes in the Fermi level. Neglecting the temperature dependence of vibrational contributions, Eqs. [9] and [10] show that both $\varepsilon_{O_2}^{oxide}$ and $s_{O_2}^{oxide}$ are independent of temperature.

3. EXPERIMENTAL

3.1. Sample Preparation

$La_{1-x}Sr_xCoO_{3-\delta}$ powder was prepared by thermal decomposition of precursor complexes derived from nitrate solutions using ethylenediaminetetraacetetic acid (EDTA) as a complexing agent (21, 22). The resulting powder was milled several hours and calcined at 925°C in stagnant air for 10 h. Disks were obtained by uniaxially static pressing at 1.5 bar followed by isostatic pressing at 4000 bar. These disks were sintered at 1125°C for 10 h in air. The density of the resulting disks determined by an Archimedes method was typically 95–98% of the theoretical values taken from Ref. (23). Cylindrical samples 7.75 mm in diameter and 3 mm thick were cut from these disks for coulometric titration experiments.

3.2. Coulometric Titration Experiments

The measurements were performed with the electrochemical cell shown in Fig. 2, which was described previously in Refs. (13, 24). A cylindrically shaped disk of $La_{1-x}Sr_xCoO_{3-\delta}$ ($x = 0.4$ or $x = 0.7$) was enclosed in an electrochemical cell with an internal volume of approximately 250 mm^3. ZY13 ($Zr_{0.87}Y_{0.13}O_{1.935}$) solid electrolyte was used to pump oxygen into or out of the cell and to

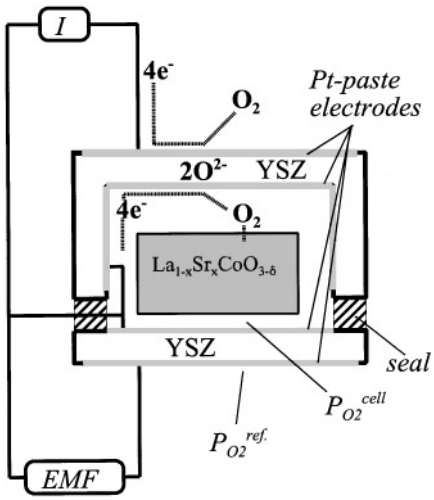

FIG. 2. Electrochemical cell used for coulometric titration experiments.

measure the EMF. Air ($P_{O_2} = 0.209$ bar) was used as reference gas.

Two types of measurements were performed. In the first type, potentiostatic steps of typically 25 mV in magnitude were applied between 0 and 200 mV at various temperatures in the range 650–950°C. The change in oxygen nonstoichiometry $\Delta\delta$ corresponding to a change in the equilibrium value of P_{O_2} of the atmosphere surrounding the sample was calculated by numerical integration of the decay current according to Eq. [3]. The final value of $\Delta\delta$ was taken as the arithmetic mean of those obtained from reduction and oxidation steps. The difference was in all cases below 5×10^{-4}. No corrections were applied for the change in oxygen concentration of the gas inside the cell with each potentiostatic step. The nonstoichiometry exhibited by $La_{0.3}Sr_{0.7}CoO_{3-\delta}$ at 800°C in equilibrium with air was taken as the reference point. From a thermogravimetric study by Mizusaki *et al.* (4), this value was estimated to be $\delta = 0.210$. The value in $La_{0.6}Sr_{0.4}CoO_{3-\delta}$ at the same conditions was estimated to be $\delta = 0.0814$, by linear interpolation of the nonstoichiometry data of $x = 0.3$ and $x = 0.5$ reported by Mizusaki *et al.* (4). A similar procedure was also performed to calculate the absolute nonstoichiometry at 900°C in equilibrium with air based on the data for δ at $x = 0.3$ and $x = 0.6$ reported by Petrov *et al.* (5). The value obtained agrees within 2% with the one obtained from the interpolation procedure at 800°C accounting for the change in δ with temperature measured in the present study. The relative positions of the δ–P_{O_2} curves obtained from the potentiostatic step measurements were determined from EMF-versus-T measurements at constant oxygen stoichiometry. The measurements described above are henceforth referred to as the voltage step method.

In the second type of experiment, the open cell EMF was measured at five different temperatures, i.e., 650, 725, 800, 875, and 950°C, at various values of the oxygen nonstoichiometry of the sample. The difference in EMF measured between two successive temperatures (at constant stoichiometry) was used to determine $\varepsilon_{O_2}^{oxide}$ and $s_{O_2}^{oxide}$ at the halfway temperature. The final values of $\varepsilon_{O_2}^{oxide}$ and $s_{O_2}^{oxide}$ were calculated by averaging those obtained from heating and cooling steps. These measurements are referred to as the temperature step method. Prior to these measurements, the oxygen stoichiometry of the sample was adjusted to a desired value by electrochemically pumping oxygen into or out of the cell. No corrections were applied for the change in oxygen concentration of the gas phase inside the cell occurring with each temperature step.

4. RESULTS AND DISCUSSION

4.1. Oxygen Nonstoichiometry

Experimental values of δ in $La_{0.8}Sr_{0.2}CoO_{3-\delta}$, $La_{0.6}Sr_{0.4}CoO_{3-\delta}$, and $La_{0.3}Sr_{0.7}CoO_{3-\delta}$ are plotted as a function of $\log(P_{O_2})$ and $\mu_{O_2}^{oxide}$ in Figs. 3, 4, and 5, respectively. Data were obtained using the voltage step method. Drawn lines in these figures indicate best fits to Eq. [8], which was derived on the basis of the itinerant electron model. Thermodynamic quantities obtained in this way are listed in Table 1. It is found that the values of S_{ox} and $g(\varepsilon_F)$ are nearly independent of composition, which supports the correctness of this model for compounds $La_{1-x}Sr_xCoO_{3-\delta}$.

For all compositions it is found that, at any given value of δ, $\mu_{O_2}^{oxide}$ is nearly independent of temperature, as shown in Figs. 3b, 4b, and 5b. The condition for equilibrium implies that $\mu_{O_2}^{oxide}$ is equal to the chemical potential of oxygen in the surrounding gas-phase $\mu_{O_2}^{gas}$. As can be judged from the expression of $\mu_{O_2}^{gas}$, given in the Appendix, the observed behavior implies that for these perovskite compositions, at constant oxygen stoichiometry, any variation in the temperature is balanced by a change in the equilibrium value of P_{O_2} of the surrounding atmosphere.

For the compounds with $x = 0.4$ and $x = 0.7$, δ decreases almost linearly with $\mu_{O_2}^{oxide}$. The diminished slope observed at the smallest values of δ for $x = 0.2$ stems from the increasing contribution of the configurational entropy of oxygen vacancies with decreasing δ. That is, for small values of δ, the entropy term $-2RT\ln(\delta/(3-\delta))$ in Eq. [8] becomes very large and, consequently, the slope in the δ-versus $\mu_{O_2}^{oxide}$ plot approaches zero.

4.2. Temperature Step Method: Partial Energy and Entropy of Oxygen

The temperature step method allows accurate determination of the thermodynamic quantities $\varepsilon_{O_2}^{oxide}$ and $s_{O_2}^{oxide}$. In Fig. 6, data from measurements at various values of δ in

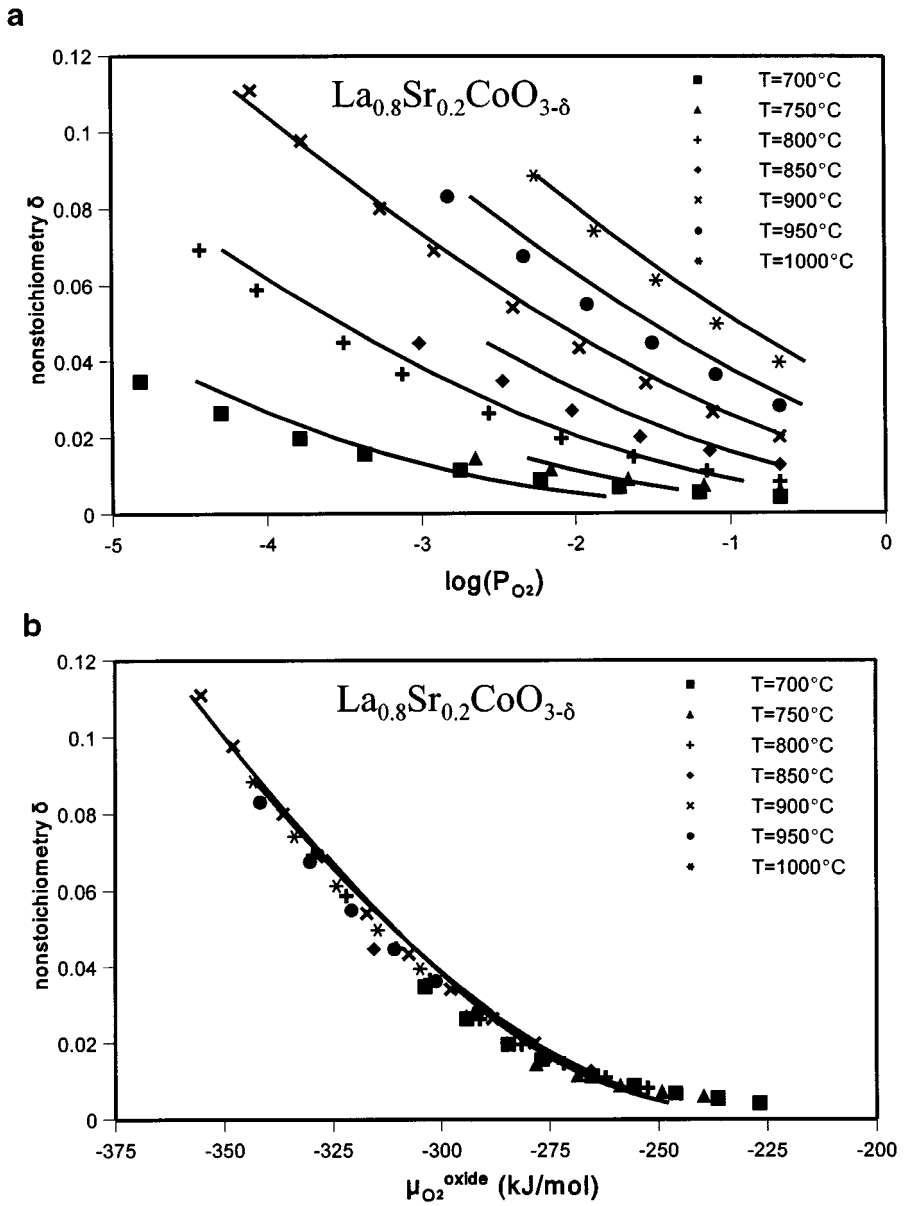

FIG. 3. Plot of the nonstoichiometry δ in $La_{0.8}Sr_{0.2}CoO_{3-\delta}$ as a function of (a) $\log(P_{O_2})$ and (b) $\mu_{O_2}^{oxide}$. Drawn lines represent best fits to the itinerant electron model (Eq. [8]).

$La_{0.3}Sr_{0.7}CoO_{3-\delta}$ are given. Similar EMF-versus-temperature plots were obtained for compositions $x = 0.2$ and $x = 0.4$. In general, good reproducibility was observed on thermal cycling. As seen from the figure, a small hysteresis is observed at the highest temperatures. This can be attributed to oxygen permeability of the zirconia electrolyte (i.e., leakage current) at these temperatures.

In Fig. 7, values of $\varepsilon_{O_2}^{oxide}$ and $s_{O_2}^{oxide}$ derived from the slopes of the EMF-versus-temperature curves are plotted as function of δ for all compositions investigated. For $La_{0.8}Sr_{0.2}CoO_{3-\delta}$, both $\varepsilon_{O_2}^{oxide}$ and $s_{O_2}^{oxide}$ are nearly independent of temperature within experimental error, which agrees with the itinerant electron model. Parameters obtained for this composition from the fitting to Eqs. [9] and [10] are listed in Table 2, showing fair agreement with those obtained from the fit of the oxygen nonstoichiometry data to Eq. [8] (Table 1). It is recalled that in the itinerant electron model one expects $\varepsilon_{O_2}^{oxide}$ to vary linearly with δ, while $s_{O_2}^{oxide}$ is described by a random distribution of oxygen vacancies. As can be seen from Fig. 7, for the compositions $x = 0.4$ and $x = 0.7$ both parameters are found to be a function of δ and temperature and therefore cannot be interpreted within the

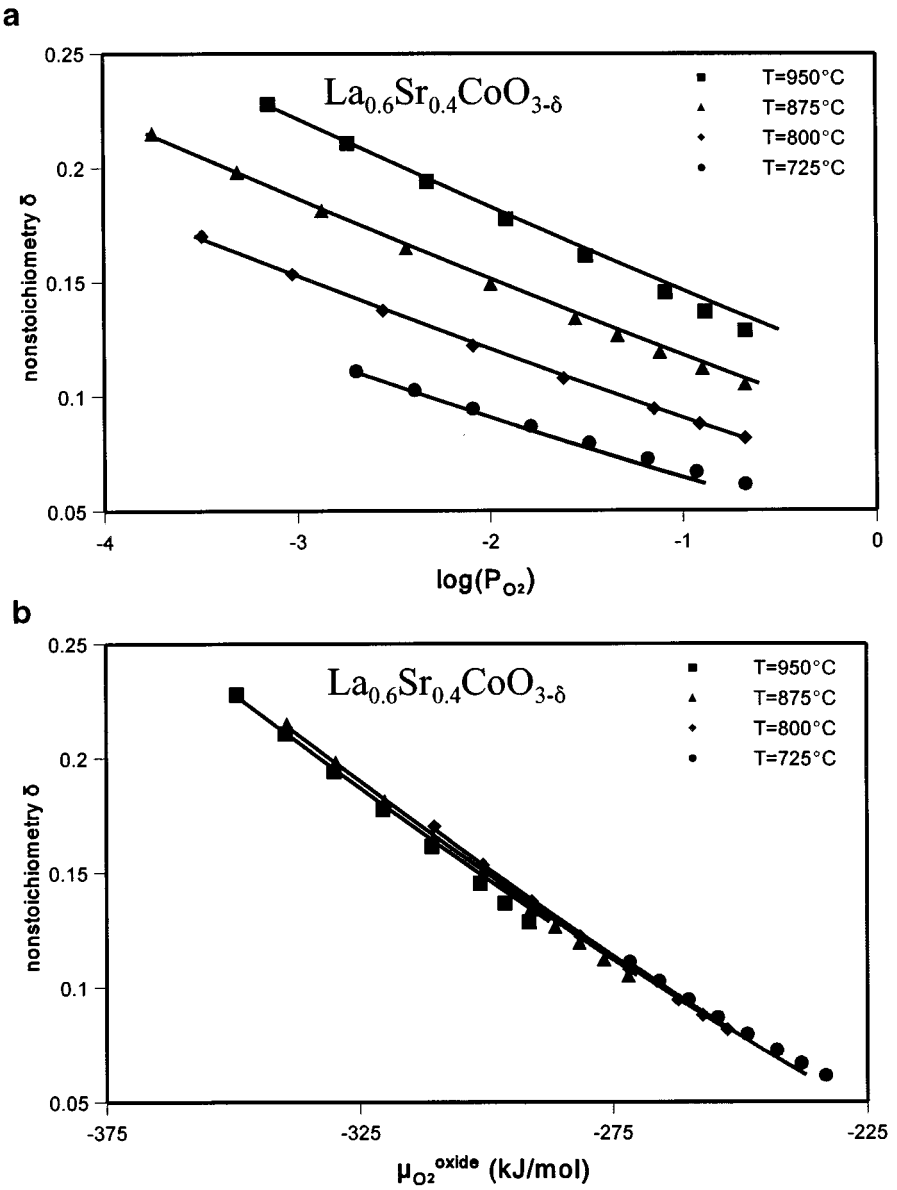

FIG. 4. Plot of the nonstoichiometry δ in $La_{0.6}Sr_{0.4}CoO_{3-\delta}$ as a function (a) $\log(P_{O_2})$ and (b) $\mu_{O_2}^{oxide}$. Drawn lines represent best fits to the itinerant electron model (Eq. [8]).

framework of the itinerant electron model. In view of the small Seebeck coefficient measured for these compounds (9), the assumption of a negligible electron entropy remains valid. This suggests that the failure of the itinerant electron model to interpret the partial energy and entropy data for the compounds $x = 0.4$ and 0.7 is due to additional ionic contributions. The observation that $\mu_{O_2}^{oxide}$ in Figs. 4 and 5 is nearly independent of temperature, whereas both $\varepsilon_{O_2}^{oxide}$ and $s_{O_2}^{oxide}$ in Figs. 7a and 7b vary with temperature, suggests that the additional energetic and entropic contributions for these compounds cancel in the expression for $\mu_{O_2}^{oxide}$. This is confirmed by the data in Fig. 8. In Fig. 8a, the equilibrium oxygen chemical potential determined at temperatures between 687.5 and 912.5°C is plotted as a function of oxygen nonstoichiometry for compounds with different Sr contents. Values were calculated from $\mu_{O_2}^{oxide} = \varepsilon_{O_2}^{oxide} - Ts_{O_2}^{oxide}$ using the data shown in Fig. 7. Although for $La_{0.3}Sr_{0.7}CoO_{3-\delta}$ a relatively small temperature influence is apparent, these results confirm that in general changes in $\mu_{O_2}^{oxide}$ with temperature are small compared with that as a function of δ or x. Figure 8b contains the same data points as presented in Fig. 8a, but now $\mu_{O_2}^{oxide}$ is plotted as a function of the net electron

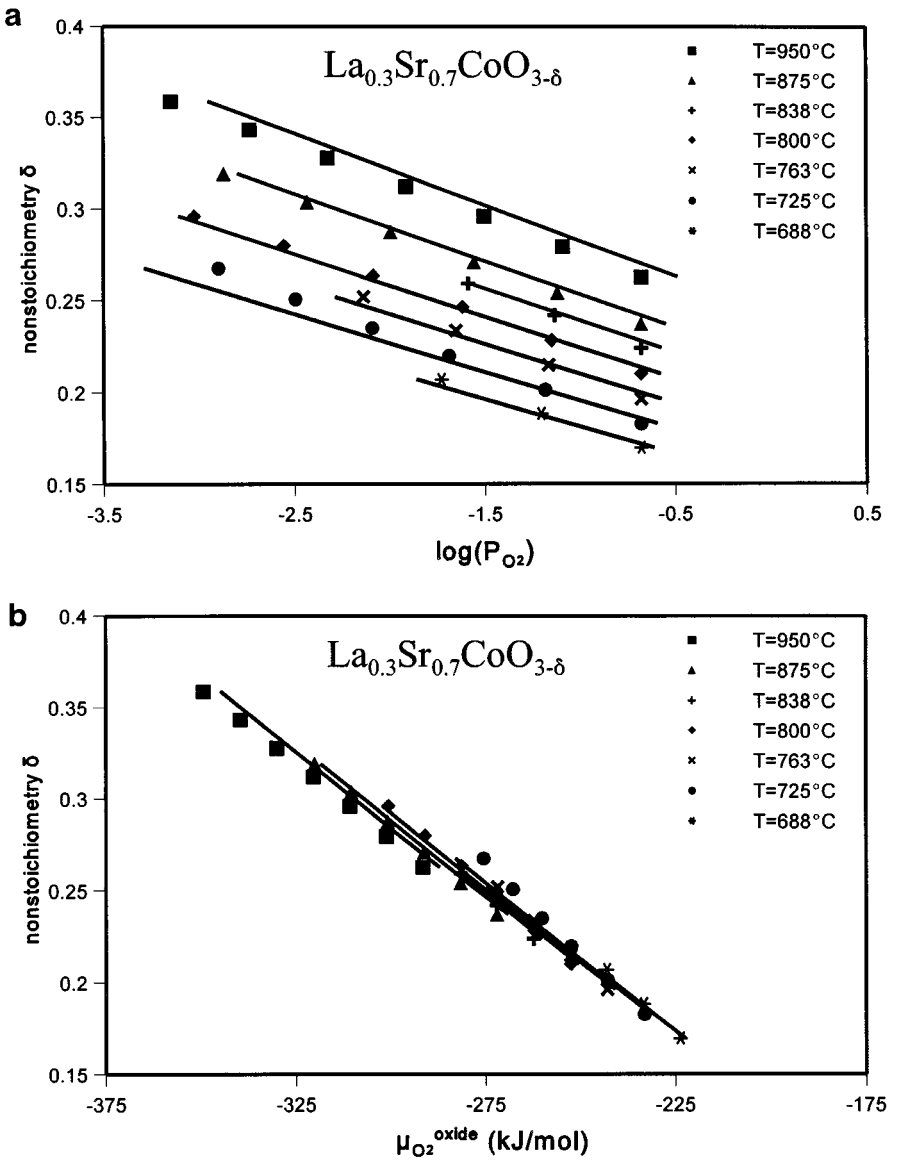

FIG. 5. Plot of the nonstoichiometry δ in $La_{0.3}Sr_{0.7}CoO_{3-\delta}$ as a function of (a) $\log(P_{O_2})$ and (b) $\mu_{O_2}^{oxide}$. Drawn lines represent best fits to the itinerant electron model (Eq. [8]).

occupancy in the band calculated from $2\delta - x$. Strikingly, all data points nearly fall onto a single line. This simple relationship between $\mu_{O_2}^{oxide}$ and the electron occupancy is to a first order of approximation independent of temperature and composition in the measured nonstoichiometry and temperature range and can be fitted using the following linear function:

$$\mu_{O_2}^{oxide}[\text{kJ/mol}] = -340 - 345 \times (2\delta - x). \qquad [11]$$

It is emphasized that this linear relationship is not valid close to the ideal stoichiometric composition due to the asymptotic behavior of the entropy of oxygen vacancies at low values of δ

Since the average valency of the La/Sr lattice increases with decreasing Sr content, the observed decrease in μ_{O_2} with decreasing x at a fixed δ might suggest that oxygen ions are more strongly bound in a lattice with less Sr. The observed decrease in μ_{O_2} with increasing δ at a fixed x might be interpreted in terms of vacancy interactions. These interpretations are based totally on ionic interactions but cannot explain the data in Fig. 8b, unless it is assumed that the variations in μ_{O_2} with x and with δ cancel. A more convincing explanation that does not rely on such a coincidence is

TABLE 1
Parameters Obtained by Fitting the Results of the Voltage Step Method to the Itinerant Electron Model (Eq. [8])

	$x = 0.2$	$x = 0.04$	$x = 0.7$
E_{ox} (kJ/mol)	− 334.1	− 301.4	− 294.5
S_{ox} (J/mol K)	69.5	69.6	70.5
$g(\varepsilon_F)$ [(kJ/mol)$^{-1}$]	0.0159	0.0159	0.0152
$g(\varepsilon_F)$ [(eV)$^{-1}$]	1.53	1.53	1.46

that the observed behavior in Fig. 8b is governed by the upward shift in Fermi level on filling up states in the band with electrons induced by vacancy formation or reducing the Sr-dopant level, i.e.,

$$\Delta\mu_{O_2}^{\text{oxide}} \approx -4\Delta\mu_{e'} = \frac{-4(2\delta - x)}{g(\varepsilon_F)}. \qquad [12]$$

That is, the electron band is taken to be rigid in the sense that it does not move as a function of changes in the composition. Such an interpretation also requires that variations in the chemical potentials of oxygen vacancies and oxygen ions on the same energy scale are small, since these are expected to vary with δ instead of $2\delta - x$. Even though energetic and entropic contributions vary with δ and temperature, as was noted from Fig. 7, these variations cancel in the ionic chemical potential.

Using Eqs. [11] and [12], the density of states at the Fermi level is calculated to be 1.1 (eV)$^{-1}$ per unit cell. This value is in good agreement with the values of 1.0, 1.3, and 1.5 (eV)$^{-1}$ obtained from the shift in the O-2p band toward the Fermi level with increasing Sr content measured using XPS by different authors (25–27). On the other hand, the screened impurity RBM would predict a constant Fermi level. Apparently, this model does not hold for compounds $La_{1-x}Sr_xCoO_{3-\delta}$.

4.3. Ionic Contributions to the Partial Energy and Entropy

As is clear from the previous sections, the assumption made in the itinerant electron model of noninteracting and randomly distributed oxygen vacancies may still be valid at low vacancy concentration, but no longer holds at high vacancy concentrations. To estimate from the experimental data shown in Fig. 7 how the energy and entropy part of $(\mu_{V_O^{\cdot\cdot}} - \mu_{O_O^x})$ depend on δ and T, we use the equations

$$\varepsilon_{V_O^{\cdot\cdot}} - \varepsilon_{O_O^x} = -\frac{1}{2}\varepsilon_{O_2}^{\text{oxide}} - 2\mu_{e'}, \qquad [13]$$

$$s_{V_O^{\cdot\cdot}} - s_{O_O^x} = -\tfrac{1}{2}s_{O_2}^{\text{oxide}}, \qquad [14]$$

where the entropy of electrons is taken to be zero. Since changes in $\mu_{e'}$ can be calculated from Eq. [7], using $g(\varepsilon_F) = 1.1$ (eV)$^{-1}$, Eq. [13] can be used to calculate changes of $(\varepsilon_{V_O^{\cdot\cdot}} - \varepsilon_{O_O^x})$ with respect to an unknown reference value. Within the approximation of zero electron entropy, Eq. [14] provides absolute values of $s_{V_O^{\cdot\cdot}} - s_{O_O^x}$. In Figs. 9a and 9b, calculated values of $\varepsilon_{V_O^{\cdot\cdot}} - \varepsilon_{O_O^x}$ and $s_{V_O^{\cdot\cdot}} - s_{O_O^x}$ are plotted as a function of oxygen nonstoichiometry and temperature.

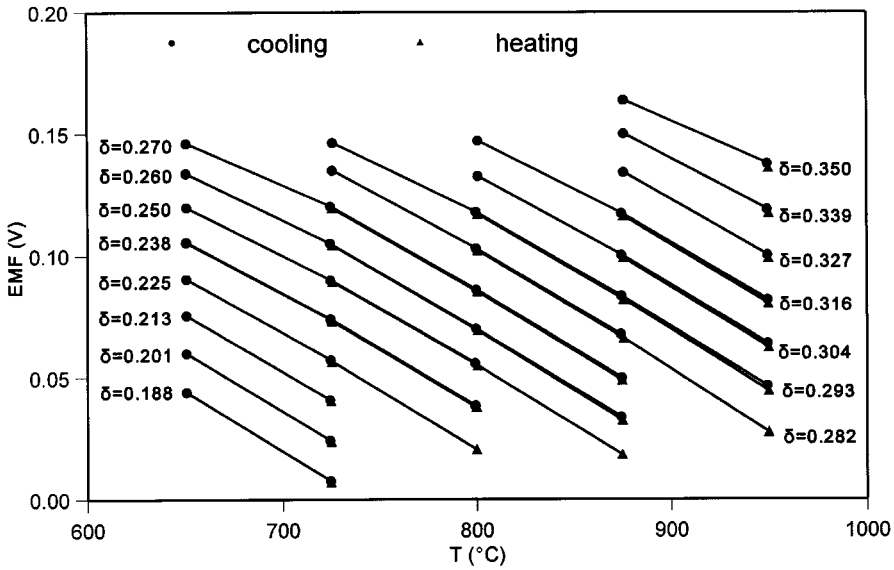

FIG. 6. Plot of the EMF versus temperature measured for various values of δ in $La_{0.3}Sr_{0.7}CoO_{3-\delta}$.

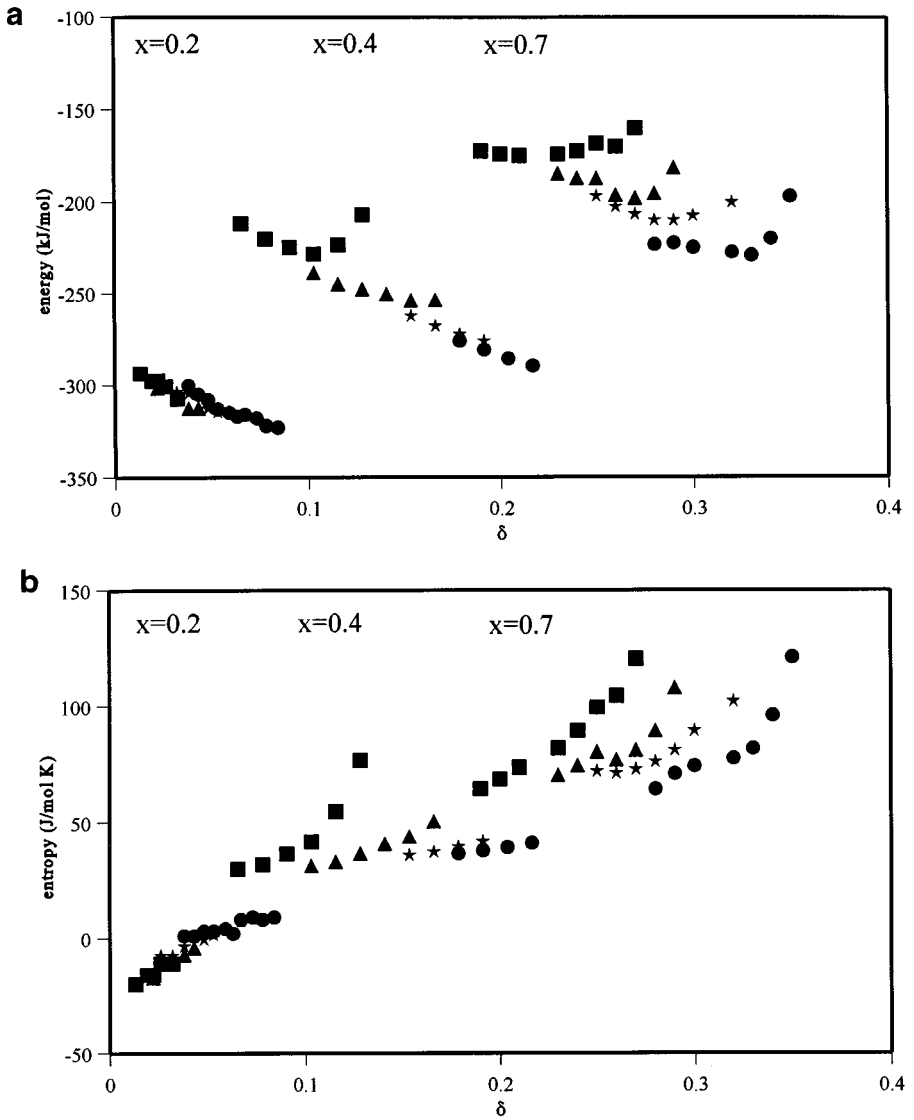

FIG. 7. Plots of (a) energy $\varepsilon_{O_2}^{oxide}$ and (b) entropy $s_{O_2}^{oxide}$ as a function of δ for $x = 0.2$ at 800°C (■), 850°C (▲), 900°C (★), and 950°C (●), and both $x = 0.4$ and 0.7 at 688°C (■), 763°C (▲), 838°C (★), and 913°C (●).

Some interesting features are observed from Fig. 9. First, both $\varepsilon_{V_O^{\cdot\cdot}} - \varepsilon_{O_O^x}$ and $s_{V_O^{\cdot\cdot}} - s_{O_O^x}$ gradually decrease with δ, while the influence of the Sr-dopant level is only small. This confirms our earlier assumption that the ionic part of the oxygen chemical potential is expected to be a function of δ. Second, the energy of lattice oxygen vacancy formation decreases with increasing δ. Since in the itinerant electron model the energy associated with oxygen vacancy formation was assumed to be constant, this explains why the values of $g(\varepsilon_F)$ obtained from fitting to the latter model are somewhat larger than that obtained from the slope of $\mu_{O_2}^{oxide}$ versus $2\delta - x$. The question remains *why* the energy of vacancy formation decreases with increasing nonstoichiometry or decreasing temperature. If repulsive coulombic defect interactions between vacancies occur, one expects the energy of oxygen vacancy formation to increase with the number of vacancies in the perovskite lattice. It is further seen from Fig. 9b that the entropy associated with vacancy formation

TABLE 2

Parameters Obtained for Composition $x = 0.2$ by Fitting Experimental Data of $s_{O_2}^{oxide}$ and $\varepsilon_{O_2}^{oxide}$ to Eqs. [9] and [10], Respectively

E_{ox} (kJ/mol)	− 330.7
S_{ox} (J/mol K)	68.7
$g(\varepsilon_F)$ [(kJ/mol)$^{-1}$]	0.018
$g(\varepsilon_F)$ [(eV)$^{-1}$]	1.91

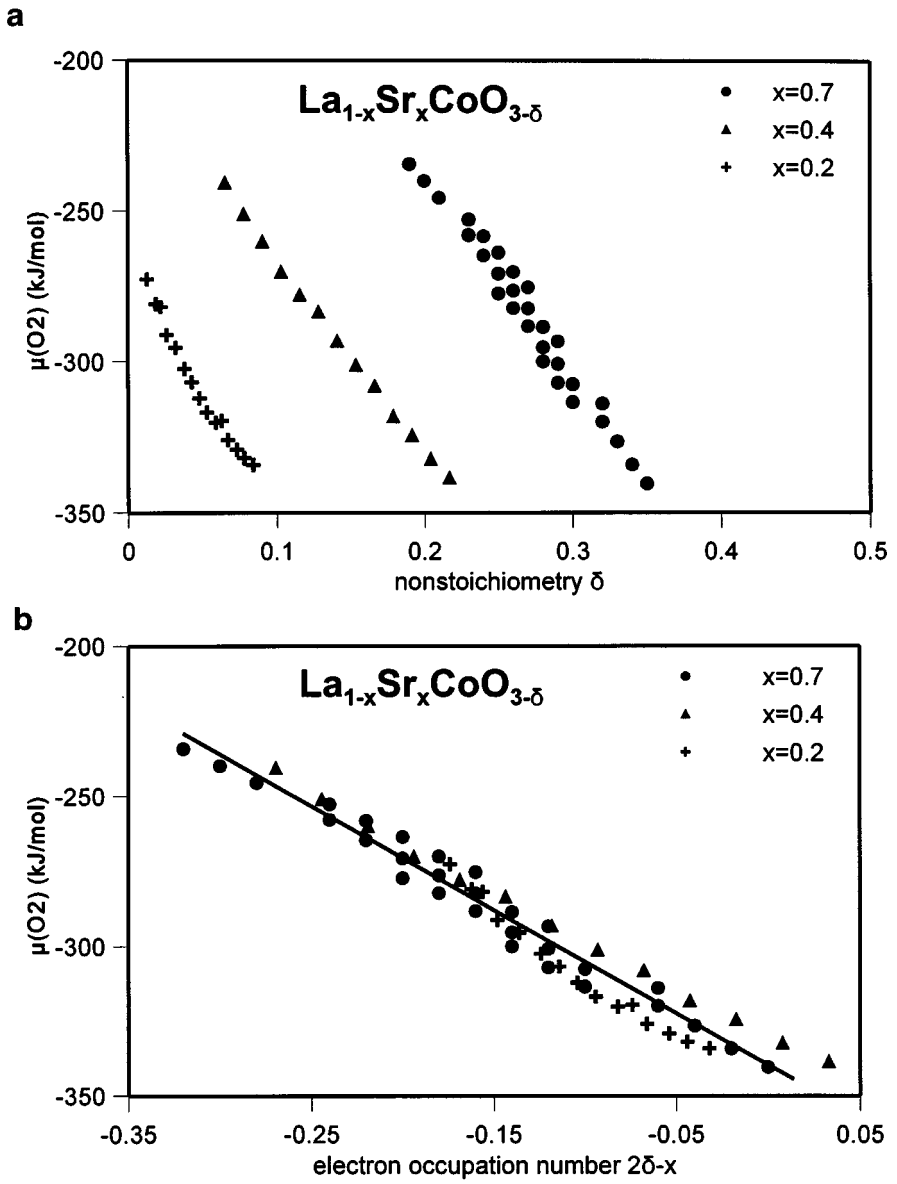

FIG. 8. Plots of $\mu_{O_2}^{\text{oxide}}$ as a function of (a) δ and (b) 2δ-x measured for $La_{1-x}Sr_xCoO_{3-\delta}$ with $x = 0.2$, 0.4, and 0.7. Data points were obtained between 687.5 and 912.5°C.

also decreases when there are more vacancies and/or when the temperature is lowered. As can be judged from the solid line in Fig. 9b, the rate at which the entropy in compositions $x = 0.4$ and 0.7 decreases is much larger than that expected for a random distribution of oxygen vacancies.

A tentative explanation for the observed behavior of $\varepsilon_{V_O^{\cdot\cdot}} - \varepsilon_{O_O^x}$ and $s_{V_O^{\cdot\cdot}} - s_{O_O^x}$ is that with increasing δ or decreasing temperature, oxygen vacancies become partially ordered into discrete islands or microdomains. Formation of the microdomains introduces a correlation between energy and entropy on the oxygen sublattice. Further, the total number of lattice sites that can be "occupied" by an oxygen vacancy is reduced compared with the random case. For the sake of illustration, the dashed line in Fig. 9b represents the entropy when oxygen vacancies are distributed over, on the average, 0.35 oxygen site per unit cell. The corresponding curve is fairly close to the experimentally observed behavior of the entropy at high δ. In this view, the data in Fig. 9 suggest that microdomain formation and the concomitant loss of accessible oxygen sites are favored at high δ and low temperature. Such an interpretation would be in agreement with observations from high-resolution TEM of microdomains with an $A_2B_2O_5$ superstructure in both furnace-cooled and quenched $La_{0.3}Sr_{0.7}CoO_{3-\delta}$

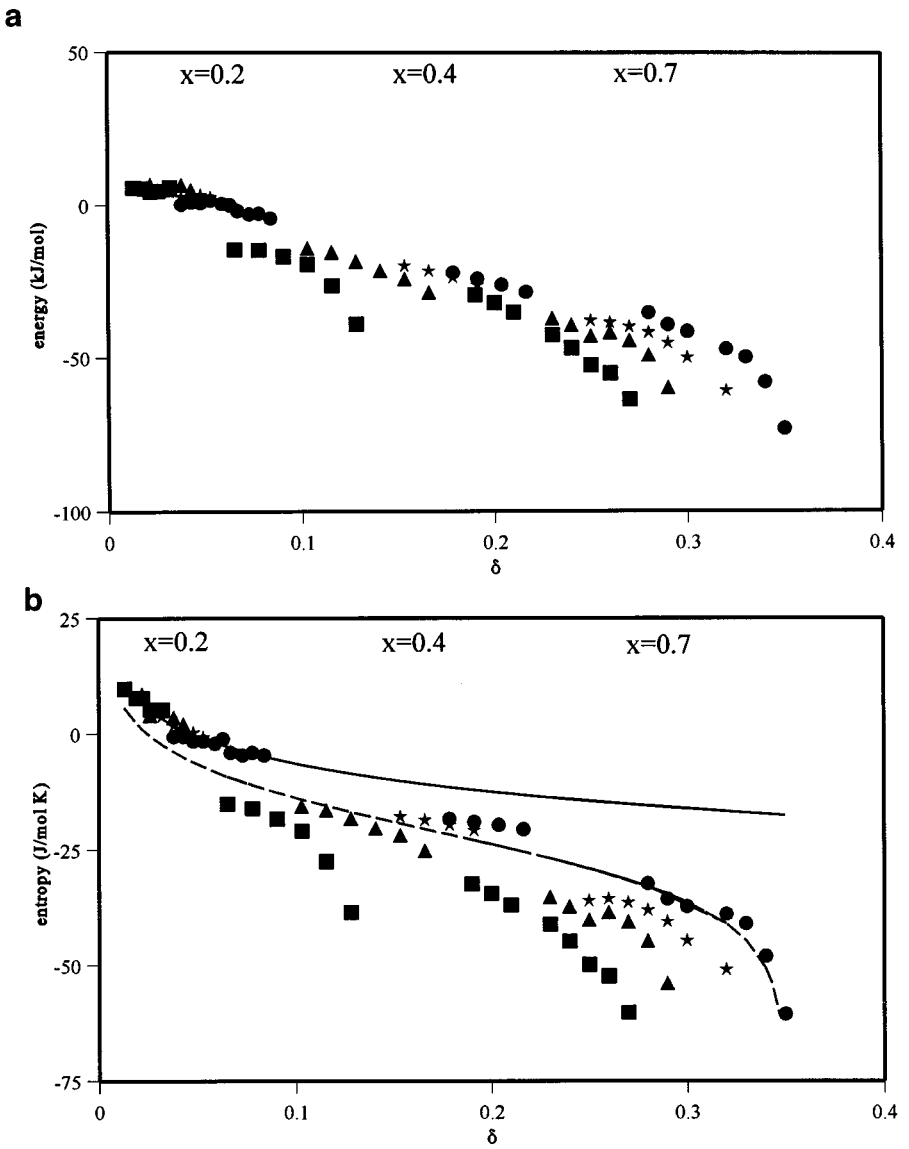

FIG. 9. Plots of (a) energy ($\varepsilon_{V_O^{\cdot\cdot}} - \varepsilon_{O_O^x}$) and (b) entropy ($s_{V_O^{\cdot\cdot}} - s_{O_O^x}$) associated with vacancy formation as a function of δ. Data points were evaluated from Eqs. [13] and [14]. Marks have the same meaning as in Fig. 7. The solid line corresponds to the random entropy of oxygen vacancies in a lattice with maximum three oxygen sites per unit cell. Similarly, the dashed line represents the case in which on the average only 0.35 oxygen site per unit cell is available.

samples (28). As a matter of fact, microdomain formation in highly defective perovskite-type oxides is frequently observed (29, 30). An important question to be addressed is whether or not the microdomains are stable at high temperatures. Unfortunately, the structural studies are usually carried out at room temperature and little is known about the extended defects at elevated temperatures Recently, however, Adler *et al.* (31) argued from data on high-temperature oxygen-17 NMR that in $La_{0.6}Sr_{0.4}Co_{0.8}Cu_{0.2}O_{3-\delta}$ below approximately 800°C only a few oxygen vacancies are mobile, while the remainder is trapped in locally ordered layers. Above 800°C, the signal intensity was found to increase steadily with temperature, suggesting a concomitant increase in the number of mobile oxygen anions.

5. CONCLUSIONS

The itinerant electron model can be used to model data of oxygen nonstoichiometry as a function of oxygen partial pressure and temperature measured for $La_{1-x}Sr_xCoO_{3-\delta}$ ($x = 0.2$, 0.4 and 0.7). It is further found that the equilibrium oxygen chemical potential of $La_{1-x}Sr_xCoO_{3-\delta}$ decreases

almost linearly with increasing net electron occupancy of the band $2\delta - x$, while its temperature dependence at constant oxygen stoichiometry is relatively small. This result can be explained in the framework of the electron gas rigid band model by assuming that electrons created during vacancy formation or decreasing the Sr content are placed in a broad electron band, inducing an upward shift of the Fermi level. Variations in the ionic chemical potential are small when viewed on the same energy scale. However, the partial energy and entropy associated with these ionic contributions do show significant variations with respect to δ and temperature, which cannot be interpreted within the itinerant electron model. These variations almost cancel completely in the expression for the oxygen chemical potential and may be due to partial ordering of oxygen vacancies into micro domains at large δ and low temperature. At low δ, the interpretation of a random distribution of oxygen vacancies remains valid.

APPENDIX: GAS-PHASE OXYGEN CHEMICAL POTENTIAL

The chemical potential of oxygen in the gas phase is given by (32)

$$\mu_{O_2}^{gas} = \mu_{O_2}^{0,gas} + RT \ln(P_{O_2})$$
$$\mu_{O_2}^{0,gas} = RT(n_1 + n_2/T + n_3 \ln(T) + n_4 \ln(1 - e^{-n})) \quad [A.1]$$

where T is in degrees Kelvin, P_{O_2} in atmospheres, atm and

$$n_1 = -1.225$$
$$n_2 = -1.045{*}10^3 \text{ K},$$
$$n_3 = -3.500$$
$$n_4 = 1.013,$$
$$n_5 = 2.242{*}10^3 \text{ K}.$$

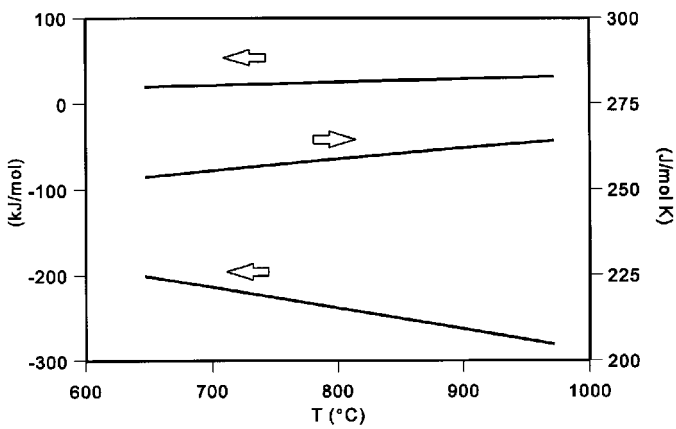

FIG. 10. Standard chemical potential of O_2 (gas), $\mu_{O_2}^{0,gas}$, and standard energy $\varepsilon_{O_2}^{0,gas}$ and entropy $s_{O_2}^{0,gas}$ of oxygen as a function of temperature. Data were evaluated from Eq. [A1].

In Fig. 10, $\mu_{O_2}^{0,gas}$ and its energy $\varepsilon_{O_2}^{0,gas}$ and entropy part $s_{O_2}^{0,gas}$ are plotted as a function of temperature. Since the value of $\mu_{O_2}^{0,gas}$ is determined by the equilibrium with the oxide sample, changes in the oxygen partial pressure with temperature result from both the temperature dependence of $\mu_{O_2}^{0,gas}$ and that of the oxygen chemical potential of the sample.

REFERENCES

1. Y. Teraoka, H. M. Zhang, S. Furukawa, and N. Yamazoe, *Chem. Lett.*, 1743 (1985).
2. H. J. M. Bouwmeester and A. J. Burggraaf, *in* "Fundamentals of Inorganic Membrane Science and Technology" (A. J. Burggraaf and L. Cot, Eds.), Ch. 10. Elsevier Science, Amsterdam, 1996.
3. R. J. H. Voorhoeve, *in* "Advanced Materials in Catalysis" (J. J. Burton and R. L. Garten, Eds.). 1977.
4. J. Mizusaki, Y. Mima, S. Yamauchi, K. Fueki, and H. Tagawa, *J. Solid State Chem.* **80,** 102 (1989).
5. A. N. Petrov, V. A Cherepanov, O. F. Kononchuk, and L. Ya. Gavrilova, *J. Solid State Chem.* **87,** 69 (1990).
6. B. C. H. Steele, *in* "Mass Transport in Oxides" (J. B. Wachtman and A. D. Franklin, Eds.), Spec. Pub. 296, p. 165. Natl. Bur. of Stand., Washington, DC, 1968.
7. M. H. R. Lankhorst, H. J. M. Bouwmeester, and H. Verweij, *J. Am. Ceram. Soc.* (1997). [in press]
8. M. H. R. Lankhorst and H. J. M. Bouwmeester, *J. Electrochem. Soc.* (1997), in press. It should be noted that in the preceding paper $[e']^0$ was defined as the electron occupancy at zero δ for the composition $x = 0.2$, whereas $[e']^0$ in the present paper is defined as the electron occupancy at zero δ for the composition $x = 0.0$. Accordingly, E_{ox} in the present study also differs from E_{ox} in the preceding paper by an amount $0.8/g(\varepsilon_F)$, *J. Electrochem. Soc.* **144**, 1268 (1997).
9. J. Mizusaki, J. Tabuchi T. Matsuura, S. Yamauchi, and K. Fueki, *J. Electrochem. Soc.* **136,** 2082 (1989).
10. L. W. Tai, M. M. Nasrallah, H. U. Anderson, D. M. Sparlin, and S. R. Sehlin, *Solid State Ionics* **76,** 273 (1995).
11. J. Mizusaki, *Solid State Ionics* **52,** 79 (1992).
12. M. Abbate, J. C. Fuggle, A. Fujimori, L. H. Tjeng, C. T. Chen, R. Potze, G. A. Sawatzky, H. Eisaki, and S. Uchida, *Phys. Rev. B* **47,** 16124 (1993).
13. M. H. R. Lankhorst and H. J. M. Bouwmeester, *J. Electrochem. Soc.* **144,** 1261 (1997).
14. F. A. Kröger and H. J. Vink, *in* "Solid State Physics" (F. Seitz and D. Turnball, Eds.), Vol. 3, p. 307. Academic Press, New York, 1956.
15. F. A. Kröger, *in* "The Chemistry of Imperfect Crystals," 2nd ed., Vol. 2, Ch. 9. North-Holland, Amsterdam, 1964.
16. D. J. Sellmyer, *in* "Solid State Physics" (H. Ehrenreich, F. Seitz, and D. Turnball, Eds.), Vol. 33, p. 83. 1978.
17. J. Rouxel, 'The electronic transfer and the formation of cationic intercalation', *in* "Solid State Ionics" (G. Nazri, R. F. Huggins, and D. F. Shriver, Eds.), Mater Res. Soc. Symp. Proc., Vol. 135, Materials Research, Pittsburgh, 1989.
18. J. R. Dahn, J. N. Reimers, T. Tiedje, Y. Gao, A. K. Sleigh, W. R. McKinnon, and S. Cramm, *Phys. Rev. Lett.* **68,** 835 (1992).
19. W. R. McKinnon and L. S. Selwyn, *Phys. Rev. B* **35,** 7275 (1987).

20. J. Friedel, *Adv. Phys.* **3,** 446 (1954).
21. J. E. ten Elshof, H. J. M. Bouwmeester, H. Verweij, *Appl. Catal. A Gen.* **130,** 195 (1995).
22. R. H. E. van Doorn, H. Kruidhof, A. Nymeyer, and L. Winnubst, *J. Mater. Chem.* [submitted]
23. R. H. E. van Doorn, in "Oxygen Separation with Mixed Conducting Perovskite Membranes," thesis, p. 81. University of Twente, Enschede, The Netherlands, 1996.
24. M. H. R. Lankhorst, H. J. M. Bouwmeester, and H. Verweij, *Phys. Rev. Lett.*, **77,** 2989 (1996).
25. D. D. Sarma and A. J. Chainani, *J. Solid State Chem.* **111,** 208 (1994)
26. J. P. Kemp, D. J. Beal, and P. A. Cox, *J. Solid State Chem.* **86,** 50 (1990).
27. A. Chainani, M. Mathew, and D. D. Sarma, *Phys. Rev. B* **46,** 9976 (1992)
28. R. H. E. van Doorn, "Oxygen Separation with Mixed Conducting Perovskite Membranes," thesis, p. 86. University of Twente, Enschede, The Netherlands, 1996.
29. C. N. R. Rao, J. Gopalakrishnan, and K. Viyasagar, *Indian J. Chem.* **23A,** 265 (1984).
30. P. Hagenmuller, M. Pouchard, and J. C. Grenier, *Solid State Ionics* **43,** 7 (1990).
31. S. Adler, S. Russek, J. Reimer, M. Fendorf, A. Stacey, Q. Huang, A. Santoro, J. Lynn, J. Baltisberger, and U. Werner, *Solid State Ionics* **68,** 193 (1994).
32. IUPAC, Commission on Thermodynamics, "Oxygen, International Thermodynamic Tables of the Fluid State—9." Blackwell Scientific, Oxford, 1987.